scientific reports

Check for updates

OPEN

Tapped-inductor bi-directional Cuk converter with high step-up/down conversion ratio and its optimum design

Hongxing Chen[1]✉, Wei-ming Lin[2]✉, Wen-ran Liu[2] & Wei He[1]✉

A bidirectional DC–DC converter is required for an energy storage system. High efficiency and a high step-up and step-down conversion ratio are the development trends. In this research, a series of bidirectional high-gain Cuk circuits was derived by combining tapped inductors and bidirectional Cuk. After analyzing and comparing the characteristics of each circuit, a bidirectional high-gain Cuk circuit with a tapped-inductor (reverse coupling) was proposed. The proposed converter has a simple structure and a high voltage gain in both the step-down (Buck) and step-up (Boost) operation modes. The voltage stress of S_2 was low. The voltage stress of S_1 was high, however, and this is a disadvantage of the proposed converter. The proposed circuit's characteristics were thoroughly examined, including the voltage gain characteristics and the design of the main parameters. We established a power loss model of the new topology, and the tapped-inductor turn ratio was optimized for high efficiency. Finally, a 400 W experimental implementation of the converter was shown to achieve efficiencies of 93.5% and 92.4% in the step-up and step-down modes, respectively. These findings verified the validity of the proposed circuit's theoretical analysis.

Because of the scarcity of fossil fuels and serious environmental issues in recent years, significant effort has been focused on the development of environmentally friendly distributed generation (DG) technologies[1]. Renewable energy, however, does not produce consistent energy because of weather conditions. Energy storage is required to provide stable power[2]. Furthermore, the voltage of a storage battery is typically low, in the 12–48 V range, whereas the voltage of a DC bus is 400 V or higher to meet the requirements of an inverter or AC grid[3]. As a result, for energy storage systems to connect a low-voltage battery to a high-voltage DC bus, a bidirectional DC–DC converter with a high step-up/step-down voltage conversion ratio is required[4]. Furthermore, these converters have been researched extensively for a wide range of industrial applications, including uninterruptible power supply systems, electric vehicles, and aviation power supplies[5]. The traditional buck-boost converter can provide a high voltage gain with a large duty ratio, which will cause considerable conduction losses because of the large current ripples. Additionally, several bidirectional DC–DC converters based on isolated topologies have been presented in the literature. These topologies require a transformer and a high number of switching devices, which increases the cost and the switching losses, in addition to requiring more complicated control schemes.

Many bidirectional DC–DC converters with a high step-up/step-down conversion ratio have been proposed to improve the voltage gain and efficiency of a converter. The cascade method was used in reference [6] to broaden the ratio range of a bidirectional converter whose gain was calculated by multiplying the gains of each level converter. The efficiency was low, however, because of the cascade, and there was an issue of instability. The proposed converter in reference [7] improved a bidirectional DC-DC converter's conversion ratio by connecting the low-voltage side in parallel and the high-voltage side in a series, but the structure of the converter was complex. Some appealing solutions, such as switched capacitors[8,9], switched inductors[10], and coupled inductors[11], have been introduced for a basic bidirectional DC/DC converter to increase the voltage conversion ratio. The proposed bidirectional bridge modular switched-capacitor-based resonant DC–DC converter achieved a high step-up/step-down conversion ratio through a switched capacitor unit[8]. However, it employed a large number of switches, and the voltage and current stresses on the switches were high due to resonance. As a result, although the circuit

[1]Fujian Engineering Research Center of Safety Control for Ship Intelligent Navigation, College of Physics and Electronic Information Engineering, Minjiang University, Fuzhou, Fujian, China. [2]Fujian Key Laboratory of New Energy Generation and Power Conversion, Fuzhou University, Fuzhou 350108, China. ✉email: chen_hongxing2115@163.com; weiming@fzu.edu.cn; Hewei11@mju.edu.cn

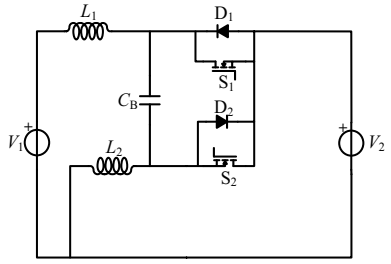

Figure 1. Bidirectional Cuk circuit.

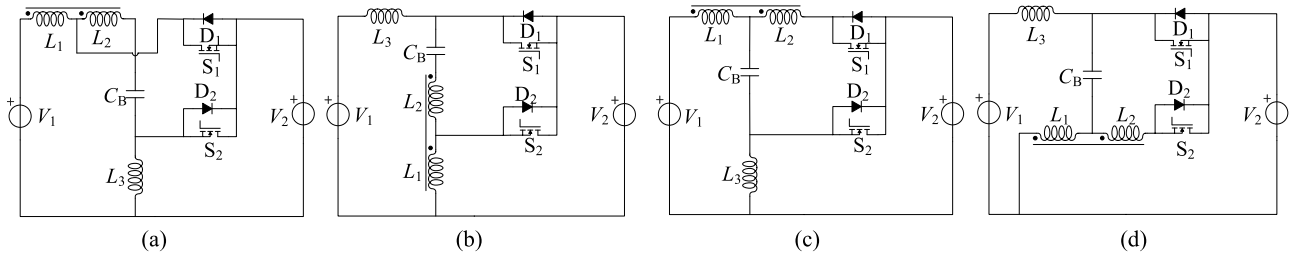

Figure 2. Bidirectional high-gain Cuk circuits are formed by the same-direction coupling, (**a**) S_1-tap, (**b**) S_2-tap, (**c**) C_B-tap 1, (**d**) C_B-tap 2.

proposed in [9] reduced the number of switches, its conversion ratio range was limited. Reference [10] employed the coupled-inductor technique to build a bidirectional DC–DC converter with a high step-up/step-down voltage gain. The current ripple was large because the current waveform on the low-voltage side of the topology was a square wave. In addition, reference [11] discussed nonisolated bidirectional DC–DC converters based on dual-coupled inductors, which could achieve a high voltage gain and reduced switch voltage stresses by connecting the secondary windings of two coupled inductors in series. However, it necessitated a complex control.

In summary, these isolated converter structures usually have too many switches, so the conduction losses of the switches were very high. Additionally, the practical implementation is complicated and expensive. The existing nonisolated high-gain circuits are mainly switch capacitor converters and coupled inductor converters. The drawbacks of a switch capacitor converter include the switching loss and the current stress. The drawbacks of a coupled inductor converter include the complex circuit structure and the leakage inductance that results in spikes that need to be suppressed using snubber circuits.

Cuk converters are gaining popularity because the input and output inductors reduce electromagnetic interference problems and the output ripple is small[12]. In this research, tapped inductance and bidirectional Cuk are combined to create a series of bidirectional high-gain Cuk circuits. After analyzing and comparing the characteristics of each circuit, a bidirectional high-gain Cuk circuit with a tapped-inductor (reverse coupling) is proposed. The proposed converter has a simple structure and high voltage gain in both the step-down (Buck) and step-up (Boost) operation modes. The proposed circuit's characteristics, including the voltage gain characteristics and the design of the main parameters, are thoroughly examined. Based on this examination, we established a power loss model of the new topology, and the tapped-inductor turn ratio was optimized for high efficiency. Finally, a 400 W 48 V/400 V prototype was created to verify the validity of the proposed circuit's theoretical analysis.

A tapped-inductor bidirectional Cuk

The bidirectional Cuk circuit features low input and output ripple and low EMI interference, and the circuit diagram is shown in Fig. 1. Because of the influence of the parasitic parameters, the voltage gain of this circuit is limited, and it is not suitable for occasions with a large voltage transformation ratio. Therefore, a series of bidirectional high-gain Cuk circuits is created by combining tapped inductance and bidirectional Cuk to increase the voltage gain of bidirectional Cuk.

The proposed series of circuits use coupled inductors to replace the inductors L_1 or L_2 in Fig. 1. Because of the different connection methods of the coupled inductor, four different circuits can be derived. Additionally, because the coupled inductor has two coupling modes (i.e., same-direction coupling and reverse-direction coupling), a total of eight circuits can be derived, as shown in Figs. 2 and 3. These converters with tapped inductors are formed by the same-direction coupling shown in Fig. 2. The reverse-direction coupling is shown in Fig. 3. The tapped inductor is composed of L_1 with the number of turns N_1 and L_2 with the number of turns N_2, where the tap ratio is $n = N_2$: N_1. Furthermore, D_1 is the parasitic body diode of S_1 and D_2 is the parasitic body diode of S_2. The same-direction coupling means that the currents all flow from the same-named end of the inductor and vice versa.

The voltage gain M of these converters versus the duty ratio D and the turn ratio n is obtained for the continuous current mode (CCM) mode by analyzing the working principles of the previously noted circuits, as shown in Table 1. S_1-tap means that the inductor L_1 of the bidirectional Cuk circuit is replaced by the tap inductor L_t, and the common terminal of the tapped inductor is connected to S_1, as shown in Fig. 2a and Fig. 3a. S_2-tap means

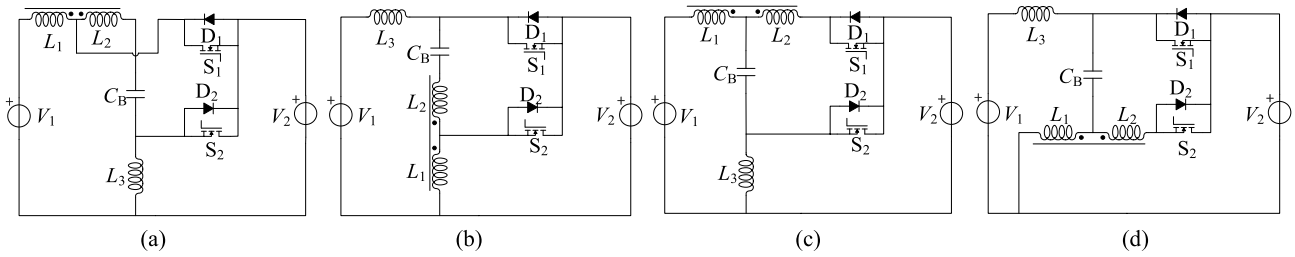

Figure 3. Bidirectional high-gain Cuk circuits are formed by the reverse-direction coupling, (**a**) S_1-tap, (**b**) S_2-tap, (**c**) C_B-tap 1, (**d**) C_B-tap 2.

Circuit	S_1-tap (same coupling)		S_2-tap (same coupling)		C_B-tap 1 (same coupling)		C_B-tap 2 (same coupling)	
	Buck (V_2/V_1)	Boost (V_1/V_2)	Buck (V_2/V_1)	Boost (V_1/V_2)	Buck (V_2/V_1)	Boost (V_1/V_2)	Buck (V_2/V_1)	Boost (V_1/V_2)
Voltage gain	$\frac{(1+n)D}{1-n(1-D)}$	$\frac{1-n(1-D)}{(1+n)(1-D)}$	$\frac{D}{1+n(1-D)}$	$\frac{1+nD}{1-D}$	$\frac{D}{1+n(1-D)}$	$\frac{1+nD}{1-D}$	$\frac{(1+n)D}{1-n(1-D)}$	$\frac{1-n(1-D)}{(1+n)(1-D)}$
Circuit	**S_1-tap (reverse coupling)**		**S_2-tap (reverse coupling)**		**C_B-tap 1 (reverse coupling)**		**C_B-tap 2 (reverse coupling)**	
	Buck (V_2/V_1)	Boost (V_1/V_2)	Buck (V_2/V_1)	Boost (V_1/V_2)	Buck (V_2/V_1)	Boost (V_1/V_2)	Buck (V_2/V_1)	Boost (V_1/V_2)
Voltage gain	$\frac{(1-n)D}{1-nD}$	$\frac{1-n(1-D)}{(1-n)(1-D)}$	$\frac{D}{1-n(1-D)}$	$\frac{1-nD}{1-D}$	$\frac{D}{1-n(1-D)}$	$\frac{1-nD}{1-D}$	$\frac{(1-n)D}{1-nD}$	$\frac{1-n(1-D)}{(1-n)(1-D)}$

Table 1. The voltage gain M versus duty ratio D and the turn ratio *n*.

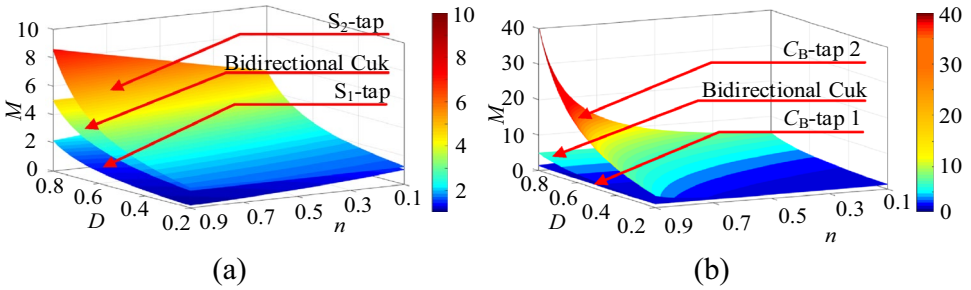

Figure 4. The voltage gain characteristic curves of the eight circuits in the step-up mode, (**a**) the same-direction coupling, (**b**) the reverse-direction coupling.

that the inductor L_2 of the bidirectional Cuk circuit is replaced by the tap inductor L_t, and the common terminal of the tapped inductor is connected to S_2, as shown in Figs. 2b and 3b. C_B-tap 1 means that the inductor L_1 of the bidirectional Cuk circuit is replaced by the tap inductor L_t, and the common terminal of the tapped inductor is connected to C_B, as shown in Figs. 2c and 3c. C_B-tap 2 means that the inductor L_2 of the bidirectional Cuk circuit is replaced by the tap inductor L_t, and the common terminal of the tapped inductor is connected to C_B, as shown in Figs. 2d and 3d.

The corresponding curve can be drawn using the data from Table 1, as shown in Fig. 4. The voltage-gain characteristic curve of the circuits formed by same-direction coupling is shown in Fig. 4a. The curves of the S_1-tap circuit and capacitor-tap circuit 2 are overlapped, and the curves of the S_2-tap circuit and capacitor-tap circuit 1 are overlapped. As shown in Fig. 4a, the bidirectional Cuk circuit with the tapped inductor derived from S_2-tap and capacitor-tap circuit 1 can achieve a high voltage gain. The voltage conversion ratio characteristic curve of the circuits formed by the reverse-direction coupling is shown in Fig. 4b. The curves of the S_1-tap circuit and capacitor-tap circuit 2 are overlapped, and the curves of the S_2-tap circuit and capacitor-tap circuit 1 are overlapped. As shown in Fig. 4b, the bidirectional Cuk circuit with the tapped inductor derived from S_1-tap and capacitor-tap circuit 2 can achieve a high voltage gain.

The voltage conversion ratio characteristic curves of the circuits in Figs. 3d and 2b are plotted, as shown in Fig. 5, to obtain the circuit with a larger step-up ratio from the previously noted circuits. As a result, it is determined that the circuit in Fig. 3d is the best of the previously noted circuits.

Because the analysis of these converters in the step-down mode is similar to the analysis in the step-up mode, it is not repeated here.

The feasibility analysis of the topologies' large ratio is shown in Table 2 based on the preceding analysis. In the table, the term "inapplicable" means that the conversion ratio of this circuit is less than that of the bidirectional Cuk circuit, and the term "available" means that the conversion ratio of this circuit is greater than that of the bidirectional Cuk circuit.

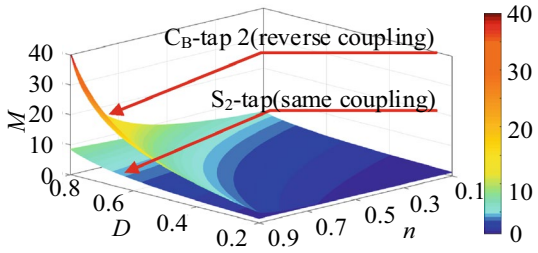

Figure 5. The voltage gain characteristic curves of the 4 circuits in step-up mode.

Circuit		The feasibility analysis
The same coupling	S_1-tap	Inapplicable
	S_2-tap	Available
	C_B-tap 1	Available
	C_B-tap 2	Inapplicable
The reverse coupling	S_1-tap	Available (high gain)
	S_2-tap	Inapplicable
	C_B-tap 1	Inapplicable
	C_B-tap 2	Available (high gain)

Table 2. The feasibility analysis of the topologies' large ratio.

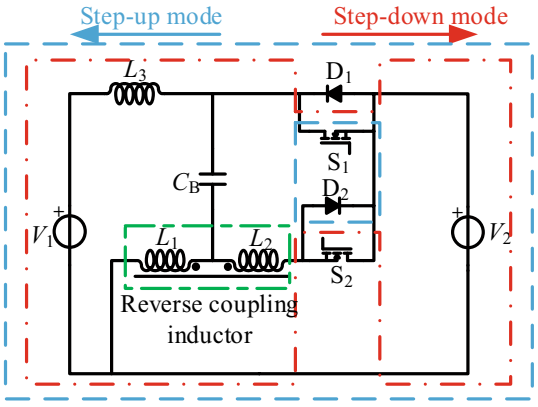

Figure 6. A reverse coupling tapped-inductor high gain bidirectional Cuk converter.

A tapped-inductor bidirectional high gain Cuk converter

The circuit topology. According to this analysis, we proposed a tapped-inductor bidirectional Cuk converter with a high step-up/step-down conversion ratio, as shown in Fig. 6. The proposed converter is made up of the following components: the low-side voltage V_2, the high-side voltage V_1, the inductor L_3, the tapped inductor L_t, the capacitor C_B, and the two switches S_1–S_2. The tapped inductor L_t is composed of L_1 and L_2 coupled in the opposite direction, and the turns of the inductor are N_1 and $N_2(N_1 > N_2)$. The equivalent circuits of these stages are shown in Fig. 7.

The effective turn ratio of the tapped inductor is expressed as follows.

$$\lambda = \frac{N_1 - N_2}{N_1} \tag{1}$$

The coupling coefficient of the tapped inductor is:

$$k = \frac{L_m}{L_m + L_k} \tag{2}$$

where L_m is the equivalent magnetizing inductance on the N_2 side; and L_k is the leakage inductance on the N_2 side.

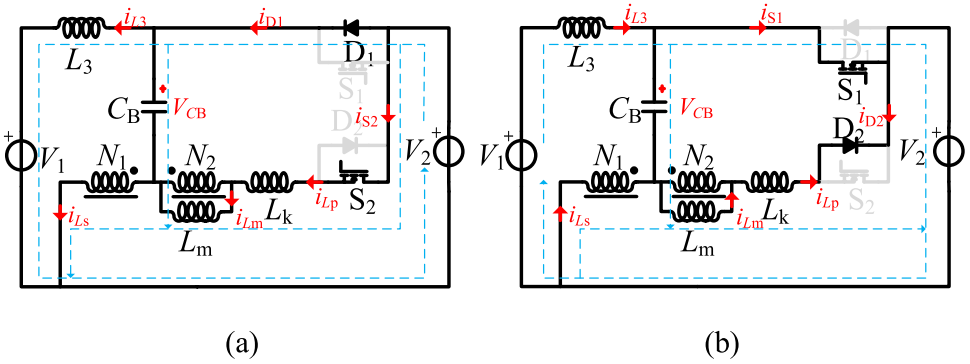

Figure 7. A reverse coupling tapped-inductor high gain bidirectional Cuk equivalent circuit, (**a**) step-up mode, (**b**) step-down mode.

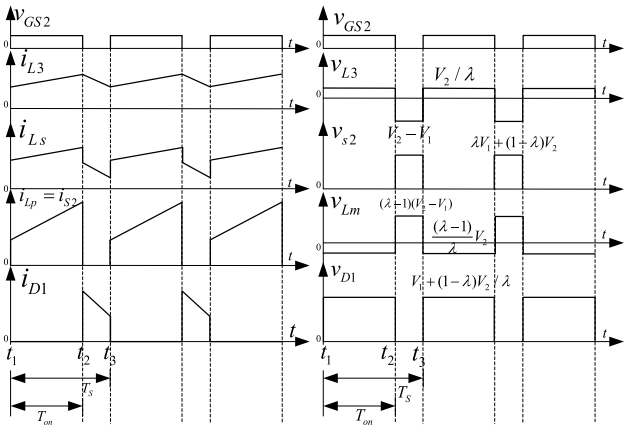

Figure 8. The main operation waveforms of the key components in the step-up mode.

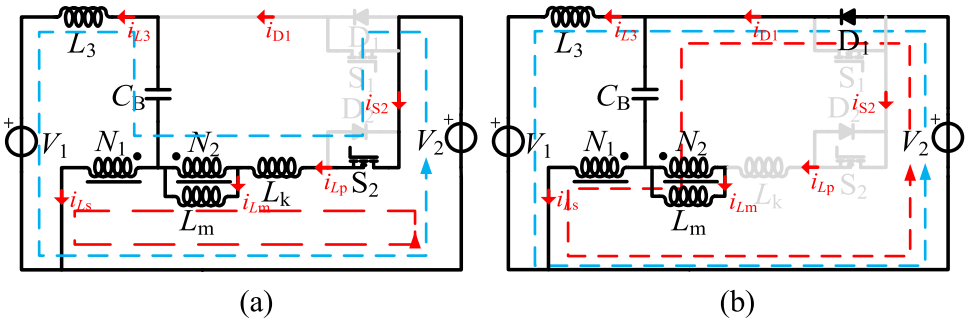

Figure 9. The equivalent circuit of the operation modes in the step-up mode, (**a**) S_2 on, (**b**) S_2 off.

Operational principles. When using the proposed circuit in energy storage systems, the battery voltage V_2 is on the low-voltage side and the DC-bus voltage V_1 is on the high-voltage side. The proposed converter can operate in both step-up mode and step-down mode with bidirectional power flow. Reference [13] contains the operating principles and steady-state analysis. Hence, the simple results are discussed in the following, but the detailed analysis is not repeated.

As shown in Fig. 8, one switching period of the step-up mode has two switching stages. In Fig. 8, v_{gs2} is the driving signal of S_2, the currents flowing through the L_1, L_2, and L_3 inductors are i_{Ls}, i_{Lp}, and i_{L3}, and i_{D1}, i_{S2}, and i_{CB} are the currents flowing through D_1, S_2, and C_B. The equivalent circuits of these stages are shown in Fig. 9.

The gain of the proposed circuit in the step-up mode can be derived as follows.

$$M_{up} = \frac{V_1}{V_2} = \frac{\lambda + (1-\lambda)D}{\lambda(1-D)} - \frac{D(1-k)}{\lambda(1-D)} \tag{3}$$

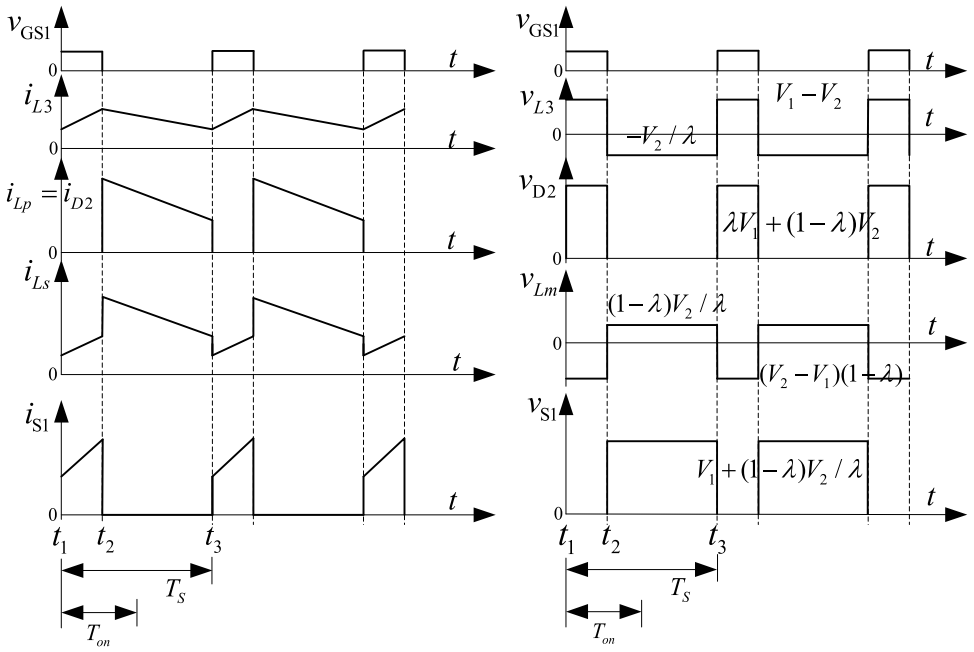

Figure 10. The main operation waveforms of the key components in the step-down mode.

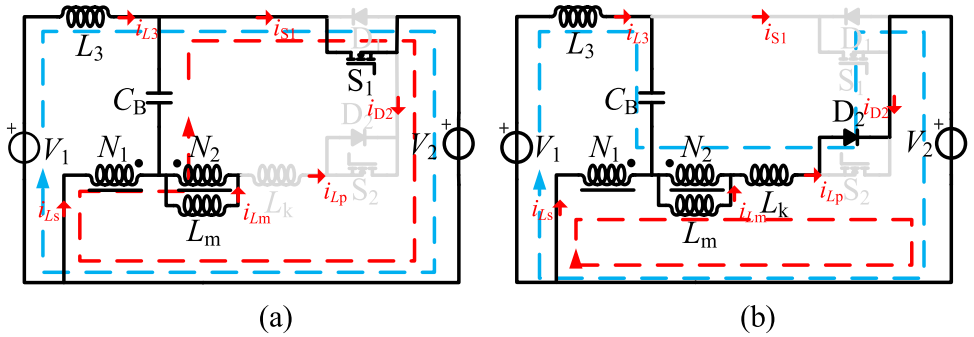

Figure 11. The equivalent circuit of the operation modes in the step-down mode, (**a**) S_1 on, (**b**) S_1 off.

Ideally, the leakage inductor can be ignored, and the M_{up} can be derived as follows.

$$M_{up} = \frac{V_1}{V_2} = \frac{\lambda + (1-\lambda)D}{\lambda(1-D)} \tag{4}$$

where M_{up} is the step-up conversion ratio of the proposed converter and D is the duty cycle of S_2.

As shown in Fig. 10, one switching period of the step-down mode has two switching stages. In Fig. 10, v_{gs1} is the driving signal of S_1, the currents flowing through the L_1, L_2, and L_3 inductors are i_{L1}, i_{L2}, and i_{L3}, and i_{D2}, i_{S1}, and i_{CB} are the currents flowing through D_2, S_1, and C_B. The equivalent circuits of these stages are shown in Fig. 11.

The gain of the proposed circuit in the step-down mode can be derived as follows.

$$M_{down} = \frac{V_2}{V_1} = \frac{\lambda D}{1 + (\lambda - 1)D} + \frac{\lambda D(1-D)(1-k)}{(1 + \lambda D - D)(k + \lambda D - kD)} \tag{5}$$

Ideally, the leakage inductor can be ignored, and M_{down} can be derived as follows.

$$M_{down} = \frac{V_2}{V_1} = \frac{\lambda D}{1 + (\lambda - 1)D} \tag{6}$$

where M_{down} is the step-down conversion ratio of the proposed converter and D is the duty cycle of S_1.

Comparison analysis of the proposed converter. The characteristic comparison of the proposed converter with the counterparts is shown in Table 3 (*NS* is the number of power switches, *NCI* is the number of

Bidirectional converter	Max. voltage stress of switches	Efficiency	Structural complexity	N_S	N_{CI}	N_I	N_C	Voltage gain	
								Step-up	Step-down
Buck/boost converter	V_H	–	Simple	2	–	1	2	$\frac{1}{1-D}$	D
The converter in [14]	V_H	88.9–92.3% (250 W)	Complex	4	1	–	3	$\frac{1}{(1-D)^2}$	D^2
The converter in [15]	$\frac{1+n}{2+n} \cdot V_H$	88.7–94.2% (400 W)	Complex	4	1	1	5	$\frac{2+n}{1-D}$	$\frac{D}{2+n}$
Proposed converter	$\frac{1}{1+(1-D)n} \cdot V_H$	89.3–93.5% (400 W)	Simple	2	1	1	2	$\frac{1-n(1-D)}{(1-n)(1-D)}$	$\frac{(1-n)D}{1-nD}$

Table 3. Characteristic comparison of the proposed converter with the main competitors.

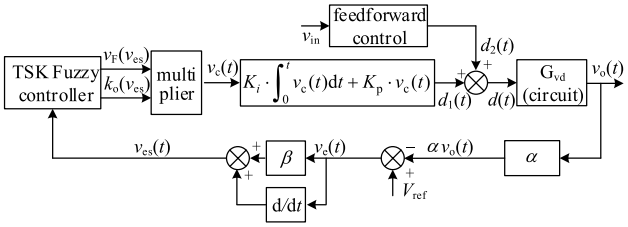

Figure 12. The improved fuzzy control schematic.

coupled inductors, *NI* is the number of inductors, and *NC* is the number of capacitors). The conventional buck/boost converter can achieve bidirectional power flows while employing the fewest number of power switches, but the converter's conversion ratio range is limited. The converter in reference [14] has a high step-up/step-down conversion ratio, but it is complex and inefficient. Compared with the converters in reference [14], the converter's efficiency in reference [15] has been improved by using soft switching technology, but the circuit structure is still complex. It can be seen that the proposed converter achieves a high and wide voltage-gain range by employing two power switches. Additionally, it has a simple structure.

The feasibly control strategy for the proposed converter. To improve the dynamic performance and antidisturbance ability of the proposed converter, we proposed an improved fuzzy control strategy based on the Takagi–Sugeno-Kang fuzzy control technique, as shown in Fig. 12. The operating principle and a detailed analysis of the control strategy can be obtained from reference [13]. Therefore, the detailed analysis is not repeated in this paper.

Analysis and design of the key parameters

Optimized design of turn ratio. *Power loss model.* A power loss model of the new topology is established in the step-up mode. The loss of the proposed converter is composed of the losses of S_2, L_t, L_3, and D_1. The specific analysis is given as follows.

(1) The loss of S_2.

The conduction loss is expressed as follows

$$P_{con\_S} = I_{rms\_S}^2 \cdot R_{ds(on)\_S} \tag{7}$$

where I_{rms_S2} is the effective value of the current across S_2, and $R_{ds(on)}$ is the forward conduction resistance of S_2 at a certain temperature, which can be estimated from the datasheet and the ambient temperature.

The switching loss is found as follows

$$P_{sw} = \frac{1}{2} \cdot f_s V_{ds} \cdot \begin{bmatrix} I_{d01} \cdot (t_{ri} + t_{fv}) \\ +I_{d02} \cdot (t_{rv} + t_{fi}) \end{bmatrix} \tag{8}$$

where t_{ri}, t_{fv}, t_r, and t_{fi} are the equivalent times of the four phases with the loss during the switching process, which can be calculated from the datasheet.

The loss of the equivalent output capacitance of S_2 is found as follows:

$$P_{Co\_S} = \frac{1}{2} \cdot C_{oss} \cdot V_{ds\_S2}^2 \cdot f_S \tag{9}$$

Therefore, the overall loss of S_2 is given by the following:

$$P_s = P_{con\_S} + P_{sw} + P_{Co\_S} \tag{10}$$

(2) The loss of D_1

$$P_D = V_F \cdot I_D + V_{off\_D} \cdot Q_{rr} \cdot f_S \tag{11}$$

where V_F is the forward voltage drop of D_1, I_D is the average value of the current across D_1, V_{off_D} is the reverse voltage of D_1, and Q_{rr} is the reverse recovery charge of D_1.

(3) The loss of the inductor

The core loss is found as follows:

$$P_{core} = f_s \cdot K f_{eq}^{\alpha-1} B^{\beta} \left(C_0 + C_1 T + C_2 T^2\right) \tag{12}$$

$$f_{eq}(D) = \frac{2}{B^2 \pi^2} \int_0^T \left(\frac{dB}{dt}\right)^2 dt = \frac{2 f_s}{\pi^2 D(1-D)} \tag{13}$$

The winding loss is found as follows

$$P_{winding} = I_{L\_rms}^2 \cdot R_{dc} \tag{14}$$

Therefore, the overall loss of inductor is given by the following:

$$P_{core} = P_{core} \cdot V_{core} + P_{winding} \tag{15}$$

where the parameters K, α, β, C_0, C_1, and C_2 can be obtained from the datasheet provided by the core manufacturer; T is the operating temperature of the magnetic core; V_{core} is the volume of the magnetic core; I_{L_rms} is the effective value of the current through the inductor; and R_{dc} is the equivalent resistance of the inductor.

The power loss models of L_t and L_3 are similar to each other. Therefore, the description of the power loss model of L_t is not repeated here.

To summarize, the overall loss of the proposed converter in the step-up mode is given by the following:

$$P_{total\_up} = P_{S2} + P_{D1} + P_{L3} + P_{Lt} \tag{16}$$

Hence, the efficiency of the proposed converter in the step-up mode is given as follows

$$\eta_{up} = \frac{P_o}{P_o + P_{total\_up}} \tag{17}$$

Similarly, the overall loss of the proposed converter in the step-down mode is given by the following:

$$P_{total\_down} = P_{S1} + P_{D2} + P_{L3} + P_{Lt} \tag{18}$$

Hence, the efficiency of the proposed converter in the step-down mode is given as follows

$$\eta_{down} = \frac{P_o}{P_o + P_{total\_down}} \tag{19}$$

The optimization selection of turn ratio. The loss characteristics of the proposed circuit are analyzed using Mathcad and the power loss model from the previous section. The following are the converter's main simulation parameters: $V_2 = 48$ V, $V_1 = 400$ V, $P_o = 400$ W, $L_3 = 1.5$ mH, $L_1 = 0.9$ mH, switching frequency: $fs = 50$ kHz.

According to Formula (16), the curves for the loss of the proposed circuit and the turn ratio under different loads can be drawn using Mathcad, as shown in Fig. 13.

From Fig. 13, when the output power is constant, the total loss of the circuit decreases at first and then increases as the turn ratio increases. As a result, a minimum loss point serves as the foundation for selecting the appropriate turn ratio in this research.

The calculation curve for the efficiency of the proposed circuit in the step-up mode can be drawn using Formula (17), as shown in Fig. 14a. Figure 14b depicts the calculation curve for the efficiency of the proposed circuit in the step-down mode, according to Formula (19).

As shown in Fig. 14, the circuit's efficiency increases at first and then decreases as the turn ratio increases. There is a maximum level of efficiency. As a result, to achieve the expected output and high efficiency, an appropriate turn ratio and steady-state duty ratio should be chosen. The turn ratio should be around 0.4, and the duty cycle should be around 0.75, according to Fig. 14.

Given the possibility of errors during the design and winding processes, the best turn ratio is λ_{opt} = 0.375–0.412. The efficiency calculation curves are shown in Fig. 15. When the proposed converter operates under rated conditions, the best turn ratio is $\lambda_{opt} = 0.394$. Figure 15a depicts the efficiency curve in the step-up mode, and Fig. 15b shows the efficiency curve in the step-down mode.

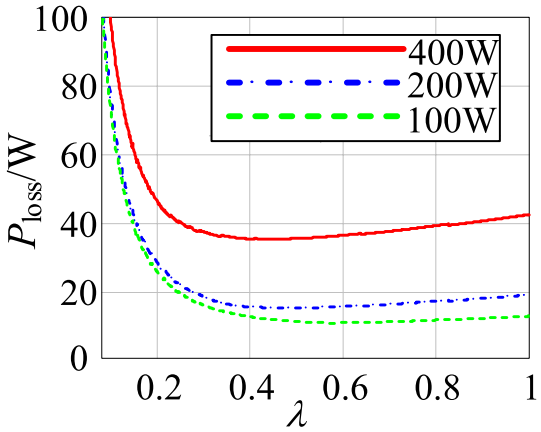

Figure 13. The curves between the loss of the proposed circuit and the turn ratio under different loads.

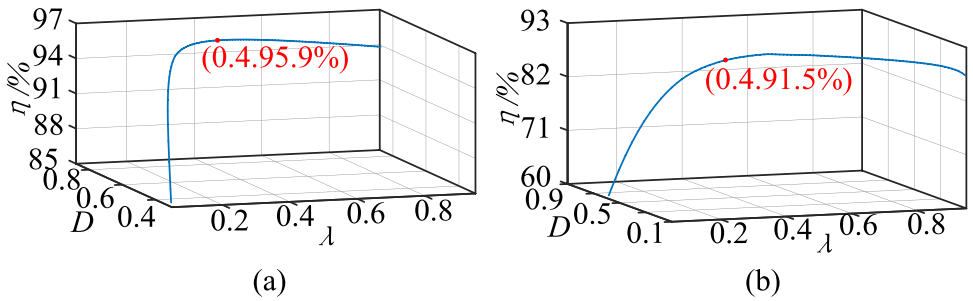

Figure 14. The calculation curve for λ, *D*, and the efficiency: (**a**) step-up mode, (**b**) step-down mode.

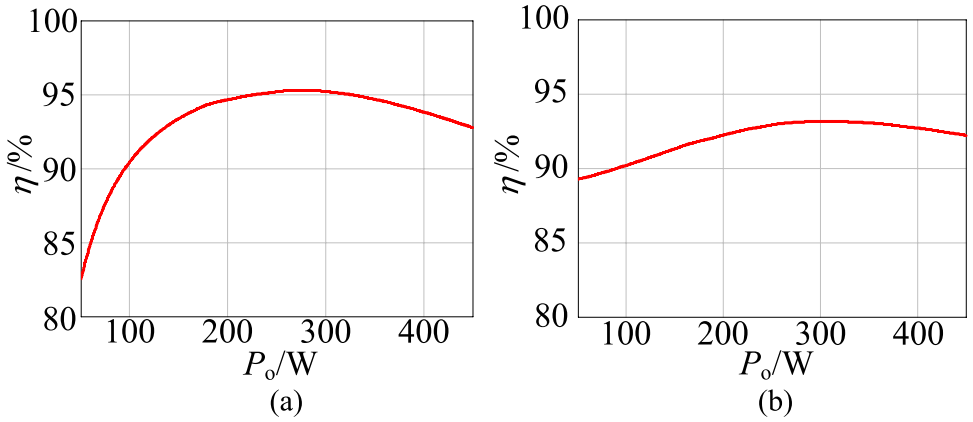

Figure 15. The calculation curve of the efficiency, (**a**)step-up mode, (**b**) step-down mode.

Other parameters design. *The selection of the inductor.* To ensure that the circuit works in CCM mode, the values of L_1, L_2, and L_3 must be greater than the inductance value with critical continuity. These values are given as follows:

$$L_1 \geq \frac{1}{\frac{2\lambda f_s I_1}{(V_1 - V_2)(1-D)} - \frac{1-\lambda}{L_3}} \tag{20}$$

$$L_2 = L_1(1-\lambda)^2 \tag{21}$$

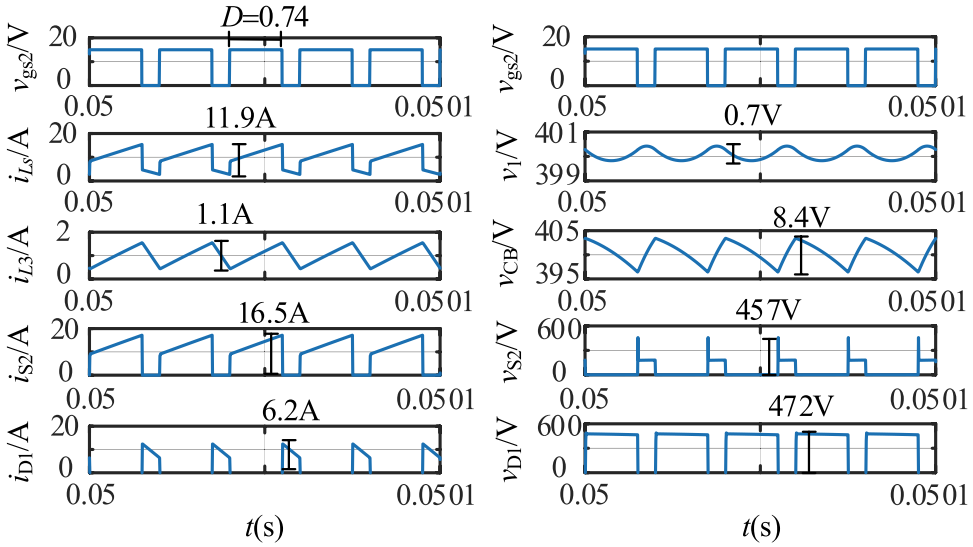

Figure 16. The stable waveforms of the key components in the step-up mode.

$$L_3 \geq \frac{V_1 - V_2}{f_s(2 \cdot I_{L3})} = \frac{V_1 - V_2}{2I_1 f_s} \tag{22}$$

The selection of capacitor. The selection of the capacitor mainly includes consideration of the voltage stress and the voltage ripple within a certain range. The value of C_B is found as follows:

$$C = \frac{|i_{CB}| \cdot DT_s}{\Delta V_C} \tag{23}$$

Simulation and experimental verification

Simulation results. We performed detailed simulations in Matlab/Simulink to verify the correctness of the aforementioned theoretical analysis. The proposed converter operation is verified at $V_2 = 48$ V, $V_1 = 400$ V, $P_o = 400$ W, $L_3 = 1.5$ mH, $L_1 = 0.9$ mH, $L_2 = 0.33$ mH, $L_k = 0.92$ uH, $C_B = 2.2$ uF, $C_{o1} = 47$ uF, $C_{o2} = 47$ uF, and the switching frequency $fs = 50$ kHz.

The simulation results in the step-up mode at full load are shown in Fig. 16. In Fig. 16, v_{gs2} is the driving signal for S_2, the currents flowing through the L_1, L_2, and L_3 inductors are i_{Ls}, i_{Lp}, and i_{L3}, and i_{D1}, i_{S2}, and i_{CB} are the currents flowing through D_1, S_2, and C_B, respectively.

The simulation results in the step-down mode at full load are shown in Fig. 17. v_{gs1} is the driving signal for S_1, the currents flowing through the L_1, L_2, and L_3 inductors are i_{Ls}, i_{Lp}, and i_{L3}, and i_{D2}, i_{S1}, and i_{CB} are the currents flowing through D_2, S_1, and C_B separately.

In the step-up mode, the output voltage is stable at 400 V, as shown in Fig. 16. The duty cycle of S_2 is 0.74. The voltage stresses of S_2 and D_1 are 457 V and 472 V. Similarly, Fig. 17 shows that the output voltage is stable at 48 V in the step-down mode. The duty cycle of S_1 is 0.26. The voltage stresses of S_1 and D_2 are 987 V and 180 V. The voltage and current spikes of S_1, S_2, and the inductor are caused by the leakage inductance of the coupled inductor. Thus, the results in Figs. 16 and 17 show that the simulation results closely match the theoretical analysis.

Experimental results. To validate the theoretical analysis, we built a laboratory prototype of the proposed converter. First, based on typical applications, we selected the operating conditions of the proposed converter as $V_2 = 48$ V, $V_1 = 400$ V, and $P_o = 400$ W. Second, according to Formulas (20)–(23), $L_3 = 1.5$ mH, $L_1 = 0.9$ mH, $L_2 = 0.33$ mH, $C_B = 2.2$ uF, $C_{o1} = 100$ uF, and $C_{o2} = 100$ uF. Then the voltage-current stress of the semiconductor device can be obtained by analyzing the specific operating principle of the converter. The voltage-current stress of S_1 is as follows:

$$\begin{cases} v_{S1.\max} = V_1 + \frac{1-\lambda}{\lambda} V_2 = \frac{1}{1+(\lambda-1)D} V_1 \\ i_{S1.\max} = \frac{\lambda}{1-(1-\lambda)D} I_2 + \frac{D(V_1-V_2)(L_1+L_3)}{2f_s L_1 L_3} \end{cases} \tag{24}$$

The voltage-current stress of S_2 is as follows:

$$\begin{cases} v_{S2.\max} = \lambda V_1 + (1-\lambda) V_2 = \frac{\lambda}{1+(\lambda-1)D} V_1 \\ i_{S2.\max} = \frac{I_1}{\lambda(1-D)} + \frac{(1-D)(V_1-V_2)(L_1+L_3)}{2\lambda f_s L_1 L_3} \end{cases} \tag{25}$$

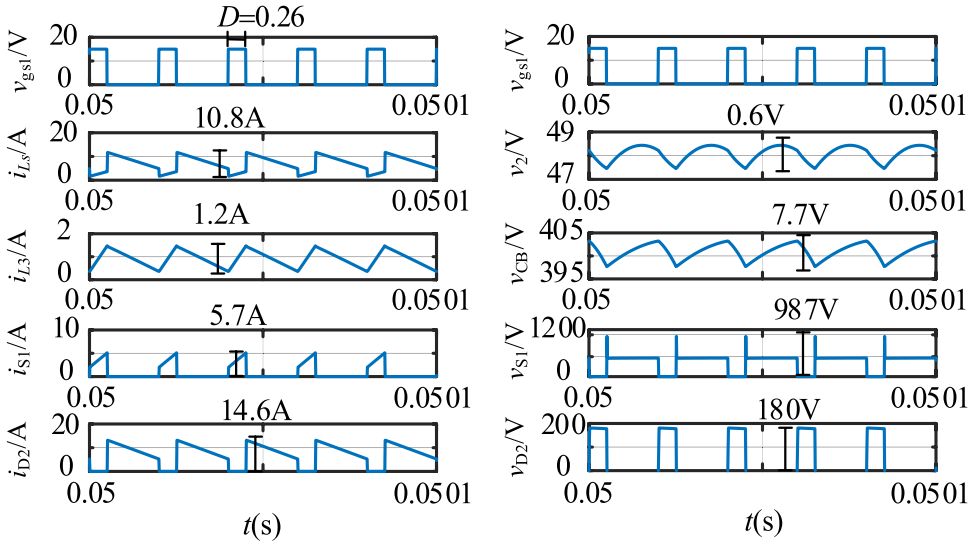

Figure 17. The stable waveforms of the key components in the step-down mode.

Parameters	The proposed converter
V_1/V	400 (250–430)
V_2/V	48 (36–60)
P_o/W	400
L_1,L_2/uH	900:346
L_k/uH	0.92
L_3/mH	1.5
C_B	2.2 uF
Co	100 uF
S_1	STP20N95K5
S_2	TK39N60W
f_s/kHz	50

Table 4. The parameters of the proposed circuit.

where I_1 is the average value of the high-voltage side current and I_2 is the average value of the low-voltage side current.

The maximum voltage and the current stress values of S_1 and S_2 are obtained by incorporating the corresponding parameters. Then, based on a certain margin, the specific type of switching tube that is required can be selected. The specific parameters of the proposed converter are listed in Table 4, and the prototype is shown in Fig. 18.

When $v_2 = 48$ V, we obtain the experimental results in the step-up mode at a full load as shown in Fig. 19. Figure 19a shows the waveforms of v_{gs2}, v_{ds2}, and i_{ds2}, and the duty cycle of S_2 is 0.75. The voltage stress of S_2 is 325 V. Figure 19b shows the waveforms of v_{gs2}, v_{D1}, and i_{D1}, and the voltage stress of D_1 is 675 V. Figure 19c shows the waveforms of v_{gs2}, v_1, i_{L1}, and i_{L3}, and the output voltage of the proposed converter in step-up mode is 400.8 V.

When $v_2 = 36$ V, we obtain the experimental results in the step-up mode at full load as shown in Fig. 20. As illustrated in Fig. 20, the duty cycle of S_2 is 0.81, and the output voltage of the proposed converter in the step-up mode is 400.4 V. The voltage stresses of S_2 and D_1 are 362 V and 669 V.

When $v_2 = 60$ V, we obtain the experimental results in the step-up mode at full load as shown in Fig. 21. As illustrated in Fig. 21, the duty cycle of S_2 is 0.69, and the output voltage of the proposed converter in the step-up mode is 400.1 V. The voltage stresses of S_2 and D_1 are 315 V and 725 V.

Compare with the simulation results in Fig. 16, the experimental results in the step-up mode are consistent with it. Both of them are then consistent with the theoretical analysis. The voltage and current spikes are caused by the leakage inductance.

When $v_1 = 400$ V, we obtain the experimental results in the step-up mode at full load as shown in Fig. 22. Figure 22a shows the waveforms of v_{gs1}, v_{ds1}, and i_{ds1}, and the voltage stress of S_1 is 731 V. Figure 22b shows the waveforms of v_{gs1}, v_{D2}, and i_{D2}, and the voltage stress of D_2 is 225 V. Figure 22c shows the waveforms of v_{gs2}, v_o, i_{L1}, and i_{L3}, and the output voltage of the proposed converter is 47.9 V.

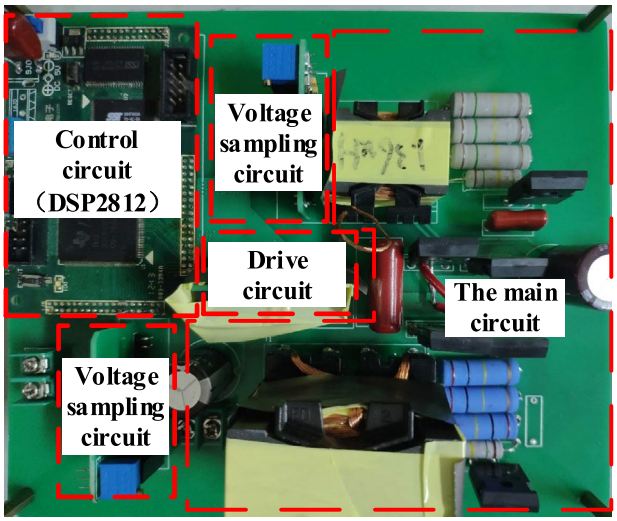

Figure 18. Prototype of the converters.

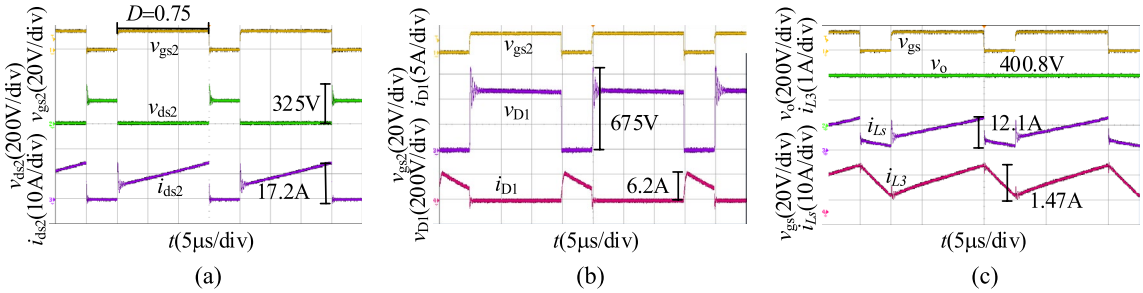

Figure 19. The experiment results of the proposed converter in the step-up mode when $v_2 = 48$ V: (**a**) v_{gs2}, v_{ds2}, i_{ds2}, (**b**) v_{gs2}, v_{D1}, i_{D1}, (**c**) v_{gs2}, v_1, i_{L1}, i_{L3}.

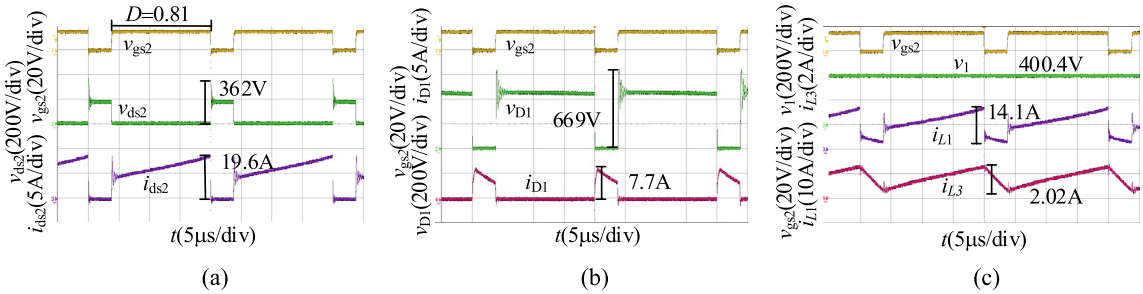

Figure 20. The experiment results of the proposed converter in the step-up mode when $v_2 = 36$ V: (**a**) v_{gs2}, v_{ds2}, i_{ds2}, (**b**) v_{gs2}, v_{D1}, i_{D1}, (**c**) v_{gs2}, v_1, i_{L1}, i_{L3}.

When $v_1 = 250$ V, we obtain the experimental results in the step-down mode at full load as shown in Fig. 23. As illustrated in Fig. 23, the duty cycle of S_1 is 0.4, and the output voltage of the proposed converter in the step-up mode is 47.9 V. The voltage stresses of S_1 and D_2 are 640 V and 173 V.

When $v_1 = 250$ V, we obtain the experimental results in the step-down mode at full load as shown in Fig. 24. As illustrated in Fig. 24, the duty cycle of S_1 is 0.253 and the output voltage of the proposed converter in the step-up mode is 47.9 V. The voltage stresses of S_1 and D_2 are 785.5 V and 245 V.

Similarly, compare with the simulation results in Fig. 17, the experimental results in the step-down mode are consistent with it. Both of them are then consistent with the theoretical analysis.

We obtain the input and output current waveforms in the step-up/step-down mode at full load as shown in Fig. 25. Figure 25a shows the current waveforms in the step-up mode, and Fig. 25b shows the current waveforms

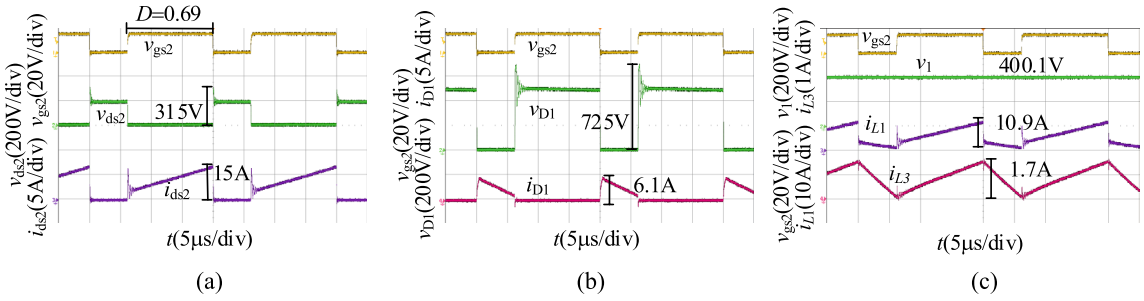

Figure 21. The experiment results of the proposed converter in the step-up mode when $v_2 = 60$ V: (**a**) v_{gs2}, v_{ds2}, i_{ds2}, (**b**) v_{gs2}, v_{D1}, i_{D1}, (**c**) v_{gs2}, v_1, i_{L1}, i_{L3}.

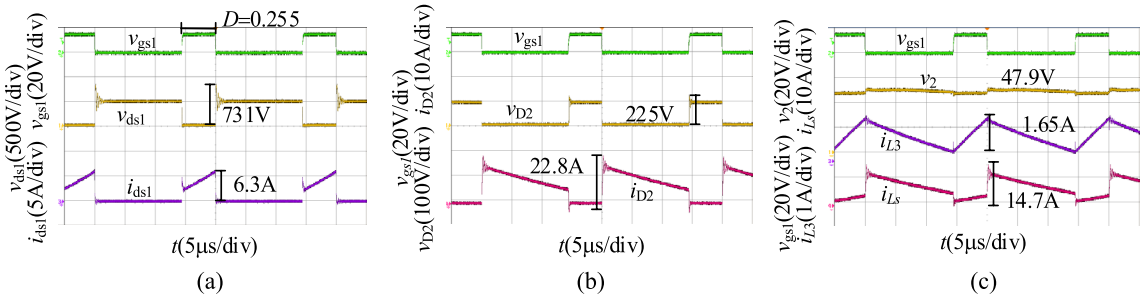

Figure 22. The experiment results of the proposed converter in the step-down mode when $v_1 = 400$ V: (**a**) v_{gs1}, v_{ds1}, i_{ds1}, (**b**) v_{gs1}, v_{D2}, i_{D2}, (**c**) v_{gs}, v_2, i_{L1}, i_{L3}.

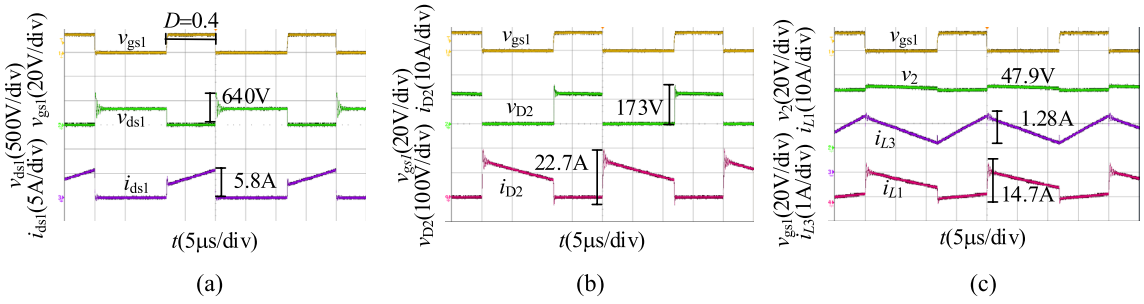

Figure 23. The experiment results of the proposed converter in the step-down mode when $v_1 = 250$ V: (**a**) v_{gs1}, v_{ds1}, i_{ds1}, (**b**) v_{gs1}, v_{D2}, i_{D2}, (**c**) v_{gs}, v_2, i_{L1}, i_{L3}.

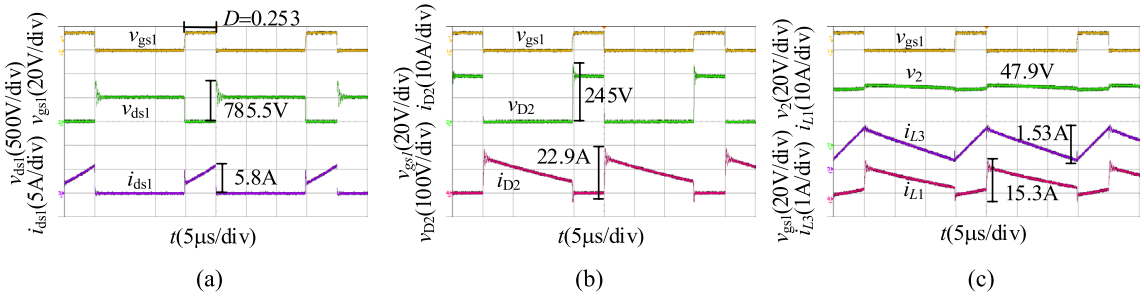

Figure 24. The experiment results of the proposed converter in the step-down mode when $v_1 = 430$ V: (**a**) v_{gs1}, v_{ds1}, i_{ds1}, (**b**) v_{gs1}, v_{D2}, i_{D2}, (**c**) v_{gs}, v_2, i_{L1}, i_{L3}.

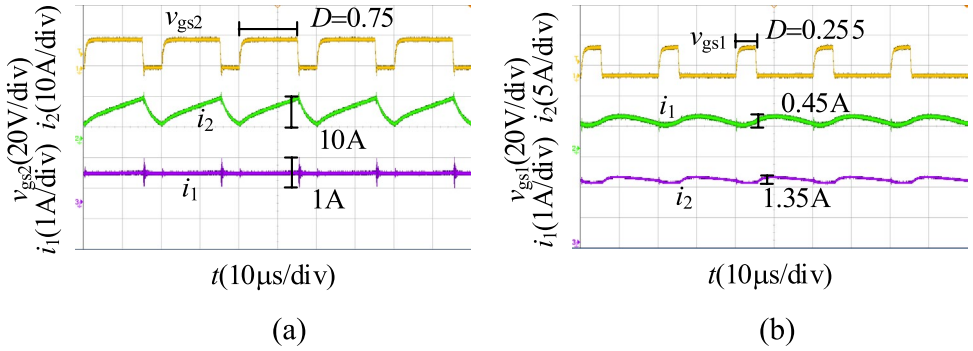

Figure 25. The input and output current waveforms of the proposed converter, (**a**) step-up mode, (**b**) step-down mode.

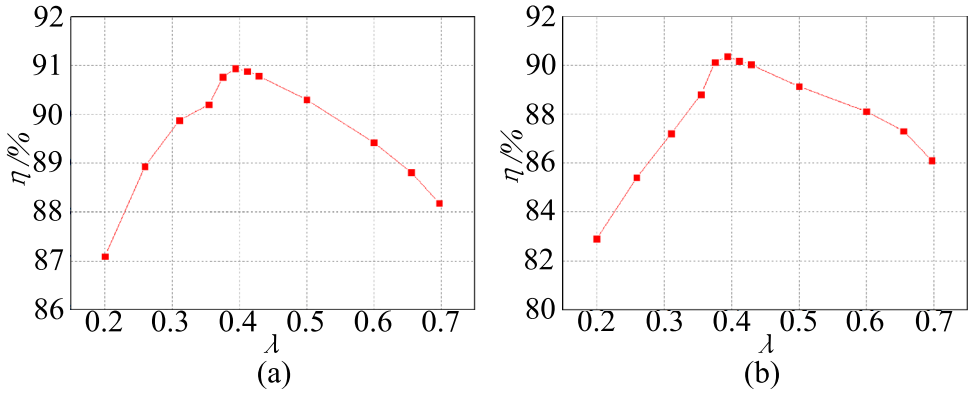

Figure 26. The efficiency curves of λ, (**a**) step-up mode, (**b**) step-down mode.

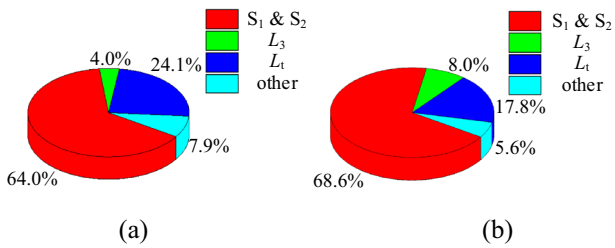

Figure 27. The experimental loss of the proposed converter, (**a**) step-up mode, (**b**) step-down mode.

in the step-down mode. As illustrated in Fig. 25, the input and output current ripple of the proposed converter is low.

The measured efficiency curve of the experimental circuit in the step-up mode is shown in Fig. 26a. Figure 26b shows the measured efficiency curve of the experimental circuit in the step-down mode. Compare with Fig. 14, it can be seen that the proposed circuit's measured efficiency curve agrees with the calculation curve. The trends of the curves are increased firstly and then decreased. Furthermore, because the actual total loss is not taken into account in the calculation, the maximum measured efficiency is less than the theoretical calculation value.

When the proposed converter operates under rated conditions and the best turn ratio is $\lambda_{opt} = 0.394$, we obtain the experimental loss of the proposed converter as shown in Fig. 27. As illustrated in Fig. 27, the loss is mainly concentrated on the switching and the coupled inductor in the step-up/step-down mode.

The conversion efficiency versus the output power in the step-up mode and step-down mode is plotted in Fig. 28.In the step-up mode, the maximum efficiency of the proposed converter is 93.5%. In the step-down mode, the proposed converter has a maximum efficiency of 92.2%.

Comparing Figs. 28 and 15, we found that the trends of the measured efficiency curve and the calculation curve ere consistent in the step-up/step-down mode. The trends increased at first and then decreased as the

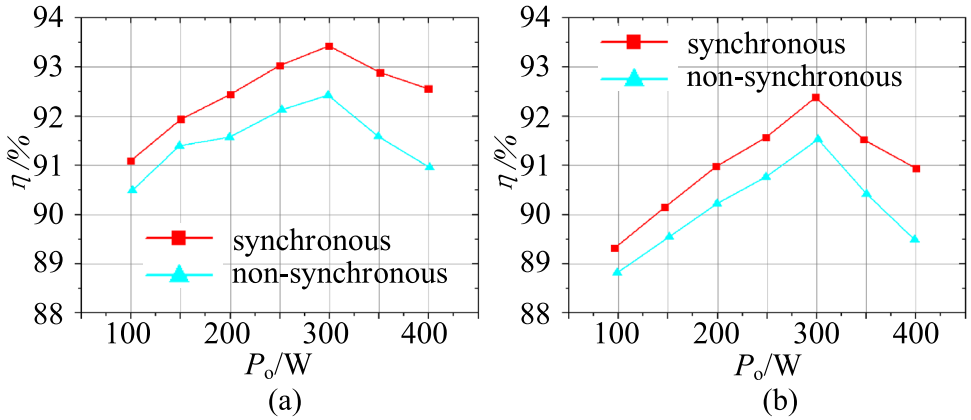

Figure 28. The efficiency curves with the load, (**a**) step-up mode, (**b**) step-down mode.

output power increased. Similarly, because the actual total loss was not taken into account, the maximum measured efficiency was less than the theoretical calculation value.

Conclusion

The use of a tapped inductor in this research improved the bidirectional DC-DC converter's conversion ratio and overcame the shortcomings of the nonisolated bidirectional DC–DC converter's low conversion ratio. Furthermore, a series of bidirectional high-gain Cuk circuits was derived by summarizing and analyzing the various forms of the proposed coupled inductor. The best circuit was obtained by analyzing and comparing the characteristics of each circuit, and we proposed a bidirectional high-gain Cuk circuit with a capacitor-tapped inductor (reverse coupling). In both the step-down and step-up operation modes, this converter had a simple structure and a high voltage gain. Following this, the proposed circuit's operational principles and characteristics were thoroughly examined. In addition, the efficiency of the proposed converter was improved further after the optimal selection of the coupled inductor's turn ratio. Finally, we created a 400 W 48 V/400 V prototype to verify the validity of the proposed circuit's theoretical analysis.

Data availability

The datasets of this study are available from the corresponding author on reasonable request.

Received: 3 May 2022; Accepted: 31 July 2022
Published online: 12 August 2022

References

1. Lai C.M., Lin, Y.C., & Lin, Y.J. Newly-constructed bidirectional DC/DC converter topology with high voltage conversion ratio for vehicle to DC-microgrid (V2DCG) system. in *2015 IEEE 2nd International Future Energy Electronics Conference (IFEEC)*. (IEEE, 2015).
2. Yamamoto, Y., Takiguchi, T., & Sato, T. *et al.* Two-phase interleaved bidirectional converter input-parallel output-series connection. in (Lee, W.-C., Hyun, D.-S., Lee, T.-K. eds.) A novel control method for three-phase PWM rectifiers using a single current sensor (ISPE 2015). *IEEE Trans. Power Electron.* **15**(5), 861–870 (2000).
3. Hongfei, Wu. *et al.* High step-up-step-down non-isolated BDC with built-in DC-transformer for energy storage systems. *IET Power Electron.* **7**(13), 2571–2579 (2016).
4. Wu, H. *et al.* High step-up/step-down soft-switching bidirectional DC–DC converter with coupled-inductor and voltage matching control for energy storage systems. *IEEE Trans. Indus. Electron.* **63**(5), 2892–2903 (2016).
5. Liu, H. *et al.* A novel reversal coupled inductor high-conversion-ratio bidirectional DC–DC converter. *IEEE Trans. Power Electron.* **2017**, 1–1 (2017).
6. Ardi, H., Reza Ahrabi, R. & Ravadanegh, S. N. Non-isolated bidirectional DC–DC converter analysis and implementation. *IET Power Electron.* **7**(12), 3033–3044 (2014).
7. Zhang, Y. *et al.* Interleaved switched-capacitor bidirectional DC-DC converter with wide voltage-gain range for energy storage systems. *IEEE Trans. Power Electron.* **33**(5), 3852–3869 (2018).
8. Ding, Y., He, L., Liu, Z. Bi-directional bridge modular switched-capacitor-based DC-DC converter with phase-shift control. in *2016 IEEE Energy Conversion Congress and Exposition. Milwaukee, USA*. (IEEE, 2016).
9. Cornea, O. *et al.* Bidirectional power flow control in a DC microgrid through a switched-capacitor cell hybrid DC-DC converter. *IEEE Trans. Indus. Electron.* **64**(4), 3012–3022 (2017).
10. Hong, C.-M. *et al. Novel bidirectional DC–DC converter with high step-up/down voltage gain. 2009 Energy Conversion Congress and Exposition* (IEEE, 2009).
11. Zhang, M., Xing, Y., Wu, H. *et al.* A dual coupled inductors-based high step-up/step-down bidirectional dc–dc converter for energy storage system. in *2017 IEEE Applied Power Electronics Conference and Exposition(APEC). Tampa, USA*. (IEEE, 2017).
12. Hongxing, C. H. E. N., Weiming, L. I. N. & Tao, Z. E. N. G. A high gain step-up Cuk circuit with scalable cell. *Proc. CSEE* **39**(23), 7013–7022 (2019).
13. Hongxing, C., Weiming, L. & Tao, Z. A novel high gain bidirectional DC–DC Cuk converter and its improved fuzzy control. *Proc. Chin. Soc. Electr. Eng.* **41**(17), 6025–6039 (2021).
14. Akhormeh, A. *et al.* High gain bidirectional quadratic DC–DC converter based on coupled inductor with current ripple reduction capability. *IEEE Trans. Indus. Electron.* **68**(9), 7826–7837 (2021).

15. Zhang, Y., Liu, H. & Li, J. A low-current ripple and wide voltage-gain range bidirectional DC–DC converter with coupled inductor. *IEEE Trans. Power Electron.* **35**(2), 1525–1535 (2019).

Acknowledgements
This work was partially supported by the National Natural Science Foundation of China(No: 52172327) and the Fujian Province Natural Science Foundation(Nos.: 2021J011028, 2020J01860) and the Fuzhou Science and Technology Plan Project (No. 2021-S-236). And we thank LetPub (https://www.letpub.com) for its linguistic assistance during the preparation of this manuscript.

Author contributions
H.X. contributed to the laboratory prototype experiments, study design, interpretation, analyses, and manuscript preparation. W.M. proposed the main idea and contributed to the study design and manuscript revision. W.R. contributed to the laboratory prototype experiments and manuscript preparation. W.H. contributed to the manuscript revision. All authors contributed to and have approved the final manuscript.

Competing interests
The authors declare no competing interests.

Additional information
Correspondence and requests for materials should be addressed to H.C., W.L. or W.H.

Reprints and permissions information is available at www.nature.com/reprints.

Publisher's note Springer Nature remains neutral with regard to jurisdictional claims in published maps and institutional affiliations.